COM-RP-MPE-DRG-174

Correcting the Correction of the Correction ... ToF & PSD

prepared by Georg Weidenspointner,

Martin Varendorff and Werner Collmar

October 9, 1997

1 Introduction

The following results on the event parameters ToF and PSD are side products of a detailed investigation of COMPTEL event data at the module and sub-module level. This study, which is still in progress, was not intended to refine the currently available ToF and PSD values. Systematic differences between individual D1 and D2 modules, and even within individual modules, however, suggest that further improvements of the current ToF and PSD data might be advantageous for our analyses.

The results of the ToF studies, at the sub-module level, are presented in Sec. 2. The investigation of the PSD distributions of the individual D1 modules is summarized in Sec. 3. A brief description of the COMPASS task `EVPTPC`, which corrects ToF and PSD values according to the findings presented in this report, can be found in Sec. 4. Finally, the potential benefit of these corrected `EVP` data for imaging analysis is discussed in Sec. 5.

2 ToF

The study of the ToF distribution at the sub-module level was performed using $\mathrm{ToF_{III}}$ (`EVP-132`) data[1], which is the highest quality ToF data presently available. $\mathrm{ToF_{III}}$ data are obtained from $\mathrm{ToF_0}$ data by correcting these raw ToF values measured onboard COMPTEL for:

- the dependence on the D1 and D2 analogue sums
- the different cable lengths of the mini-telescopes
- the dependence on the D1 and D2 temperatures
- the geometrical path length between the interaction locations in D1 and D2
- the dependence on the interaction location in the D1 modules

All these corrections are based on investigations of individual and combined mini-telescopes. Due to statistical limitations it was not possible to obtain a coherent picture of a possible dependence of the ToF value on the interaction location in D2, which was expected to be smaller than in D1 because of the smaller range of distances between the interaction location and the PMT positions in D2 (Rob van Dijk, private communication).

For the ToF study presented here the D1 and D2 modules were divided in 9 and 7 so-called localization bins of equal area, respectively. In D1 8 localization bins are located before the 8 PMTs, one localization bin covers the module center. In D2 the 7 localization bins are centered above the 7 PMTs. For each of these D1 and D2 localization bins the ToF spectrum was investigated in 7 energy intervals: 0.8-1.25 MeV, 1.25-1.65 MeV, 1.65-2.0 MeV, 2.0-2.45 MeV, 2.45-4.3 MeV, 4.3-9.0 MeV and 9.0-30.0 MeV, according to the general structure of the instrumental background in $\mathrm{E_{tot}}$.

The deviation of the $\mathrm{ToF_{III}}$ forward peak position in the individual D1 modules from the average D1 detector $\mathrm{ToF_{III}}$ forward peak position for all 7 energy ranges is depicted in the top left panel of Fig. 1. Except for D1 module 5, which will play a major role in the PSD section, the $\mathrm{ToF_{III}}$ forward peak is at the same position for all modules to a high accuracy, independent of energy. Even the "deviation" of D1-05 from the other D1 modules is very small (less than 0.1 channels). The situation is slightly worse in D2, as can be seen in the top right panel of Fig. 1. The $\mathrm{ToF_{III}}$ forward peak position deviates at most 0.4 channels between individual D2 modules. The deviation of the $\mathrm{ToF_{III}}$ forward peak position in the individual D1 localization bins from the average D1 module $\mathrm{ToF_{III}}$ forward peak position for all 7 energy ranges is depicted in the bottom left panel of Fig. 1. The "largest" deviations of 0.5 channels occur at the lowest energies, where the systematic

[1]For detailed information on ToF please refer to Rob van Dijk's PhD thesis or *Approaching the ToF resolution limit* (`COM-RP-ROL-DRG-62`) by Rob van Dijk and *Studying the ToF Spectrum as a Function of Energy Part 2: the Forward Peak Region* (`COM-RP-MPE-DRG-171`) by G. Weidenspointner and M. Varendorff. The current processing status of `EVP-132` data is summarized in *Processing EVP-132 Datasets* (`COM-RP-MPE-DRG-173`) by G. Weidenspointner and T. van Sant.

uncertainties of the ToF fits are greatest. In general, the $\mathrm{ToF_{III}}$ forward peak position is very homogeneous independent of energy - showing the excellent quality of $\mathrm{ToF_{III}}$ data for D1. In D2 the situation is considerably worse, as can be seen in the bottom right panel of Fig. 1. The $\mathrm{ToF_{III}}$ forward peak position can deviate by more than 4 channels within individual D2 modules, independent of energy!

These results were obtained by combining data from Phases 1 through 6 and thus represent the average deviations over this period of time. To assess the time dependence of these deviations the analysis was repeated for data from Phases 1 and 2 and for data from Phases 5 and 6. In general, the results for data from early and late in the mission agree quite well, the differences being less than 0.2 channels. For some localization bins, however, the difference can be as large as 0.7 channels, much larger than the statistical uncertainties of the ToF fits, which in general are less than 0.1 channel, but smaller than the magnitude of the D2 deviations. This might indicate the presence of some kind of time dependence for some localizaton bins. For the time being it is assumed that there is no time dependence.

Obviously, the scatter of the $\mathrm{ToF_{III}}$ forward peak position in the D2 localization bins results in a small, additional broadening of the $\mathrm{ToF_{III}}$ forward peak width in general. Even more important, the scatter results in an inhomogenization of the telescope response, in particular at the highest energies where a selection on a narrow ToF window from 113 to 126 (compared to the standard ToF range of 115-130) is advisible, as was shown by W. Collmar et al. (*Improved COMPTEL 10-30 MeV Event Selections for Point Sources from Inflight Data*, Proc. of the 4. Compton Symposium, 1997). Under a narrow ToF selection different fractions of the signal in each D2 localization bin are accepted, resulting in an inhomogeneous response in D2.

The scatter of the $\mathrm{ToF_{III}}$ forward peak position in the D2 localization bins was corrected as follows:

- First, the average of the $\mathrm{ToF_{III}}$ forward peak positions in all D2 modules except D2-11, 13 and 14 (having failed PMTs) was determined in each energy range (D2 module 1 was corrected separately because it was not included in the original data base, D2 module 2 was omitted completely). This defines the "standard" $\mathrm{ToF_{III}}$ forward peak position as a function of energy.

- The deviation of the $\mathrm{ToF_{III}}$ forward peak position in each D2 localization bin from the "standard" $\mathrm{ToF_{III}}$ forward peak position was determined in each energy range.

- Then the average of the deviations in each energy range was determined for each localization bin.

- Finally, these average deviations were used to correct the $\mathrm{ToF_{III}}$ values according to the D2 intercation location.

In the following, the resulting ToF values are denoted by $\mathrm{ToF_{VI}}$, adopting the ToF nomenclature introduced by Rob van Dijk.

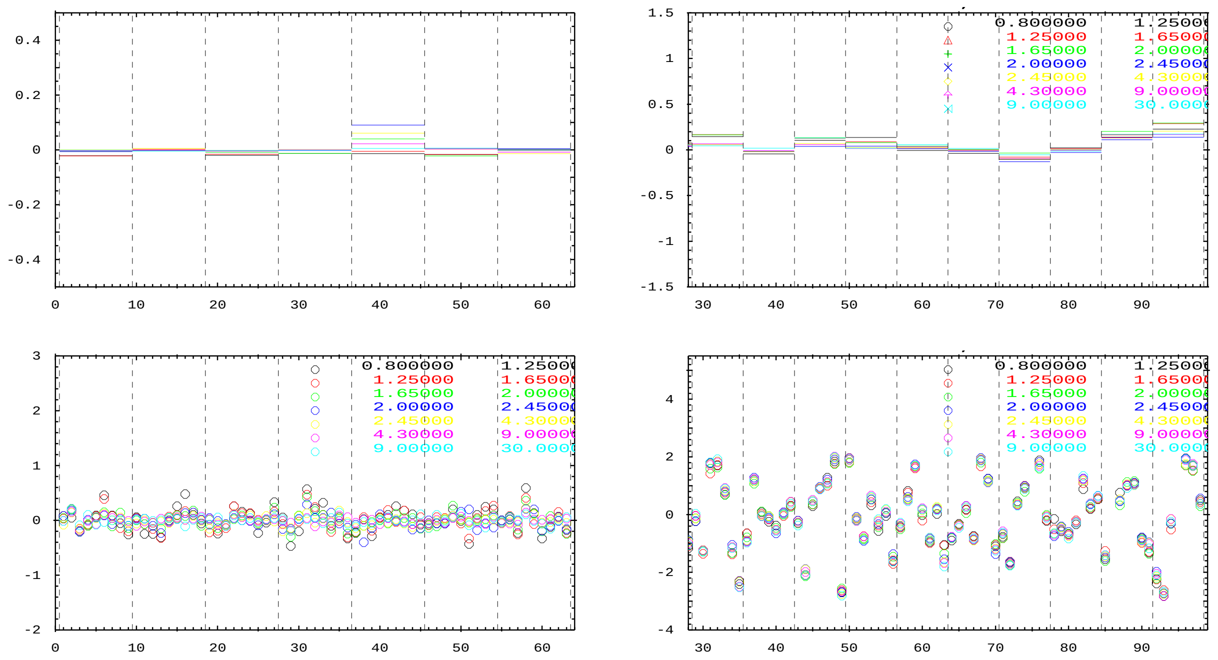

Figure 1: **Top left:** *The deviation of the* $\mathrm{ToF_{III}}$ *forward peak position in the individual D1 modules from the average D1 detector* $\mathrm{ToF_{III}}$ *forward peak position.* **Top right:** *The same as top left for D2.* **Bottom left:** *The deviation of the* $\mathrm{ToF_{III}}$ *forward peak position in the individual D1 localization bins from the average D1 module* $\mathrm{ToF_{III}}$ *forward peak position.* **Bottom right:** *The same as bottom left for D2.*

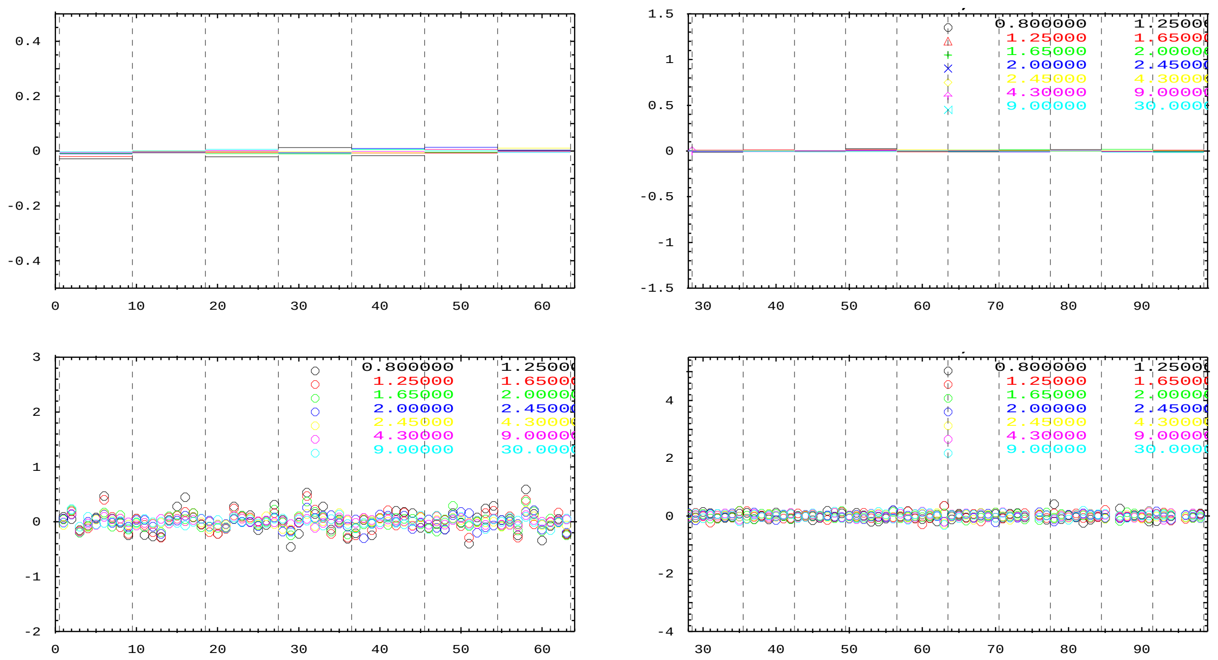

Figure 2: **Top left:** *The deviation of the* $\mathrm{ToF_{VI}}$ *forward peak position in the individual D1 modules from the average D1 detector* $\mathrm{ToF_{VI}}$ *forward peak position.* **Top right:** *The same as top left for D2.* **Bottom left:** *The deviation of the* $\mathrm{ToF_{VI}}$ *forward peak position in the individual D1 localization bins from the average D1 module* $\mathrm{ToF_{VI}}$ *forward peak position.* **Bottom right:** *The same as bottom left for D2.*

The resulting deviation of the $\mathrm{ToF_{VI}}$ forward peak position in the individual D1 and D2 modules from the average D1 and D2 detector $\mathrm{ToF_{VI}}$ forward peak position for all 7 energy ranges is depicted in the top left and right panels of Fig. 2, respectively. Now all D1 and D2 modules are very consistent (which is also true for D2-01 which is not included in the plots). The deviation of the $\mathrm{ToF_{VI}}$ forward peak position in the individual D1 and D2 localization bins from the average D1 and D2 module $\mathrm{ToF_{VI}}$ forward peak position for all 7 energy ranges is depicted in the bottom left and right panels of Fig. 2, respectively. As was to be expected, the scatter of the $\mathrm{ToF_{VI}}$ forward peak positions in D2 is now even less than in D1. As a result, the $\mathrm{ToF_{VI}}$ forward peak width (1σ) decreased from about 0.1 channels at the lowest energies to about 0.3 channels at the highest energies compared to $\mathrm{ToF_{III}}$ data, in addition to homogenizing the telescope response.

3 PSD

The (only) purpose of the event parameter PSD is to provide an efficient separation of photon and neutron events[2]. The `IFC` algorithm for the PSD correction is set up such that a corrected PSD value of 100 separates photons and neutrons best - independent of E1. It is not the aim of the PSD correction in `IFC` to provide energy independent PSD values, only the separation between photons and neutrons is intended to be independent of E1 (Cor de Vries, SRON, private communication). In the following, the raw, uncorrected PSD values measured onboard COMPTEL are denoted by PSD_0, and the corrected (standard) PSD values are denoted by PSD_I (following Rob van Dijk's nomenclature for ToF).

The PSD_0 distribution depends on the E1 analogue sum. In additon, the correlation of uncorrected PSD_0 values and E1 analogue sum is different for different D1 modules. Thus the PSD correction in `IFC` starts with fitting PSD_0 spectra as function of E1 analogue sum for each individual D1 module. With increasing energy the photon and neutron peaks tend to become narrower, at the same time they tend to come closer to each other, which may cause problems at the highest E1 energies. The final PSD corrections, however, were checked to separate photons from neutrons independent of energy. The resulting PSD_I values have been extremly stable over time ever since the launch of CGRO. Since the PSD_I distribution can be energy dependent, selections on this event parameter should be made over a relatively wide range (Cor de Vries, SRON, private communication).

The investigation of the PSD distributions of individual D1 modules was performed using standard PSD_I data (PSD_I range 0-110 channels) and was triggered by peculiarities in the E1 and Etot spectra of D1 module 5. It was recognized quickly that D1-05 was different from the other D1 modules *only* when a narrow PSD cut was applied. The PSD_I distribution as a function of E1 for D1 module 5 is depicted in the top left panel of Fig. 3. Obviously, the PSD_I distribution of this module is strongly dependent on E1 - both the photon and the neutron distributions are shifted to lower PSD_I values with increasing E1 energies. This results in a significant decrease of events from this module when a narrow PSD cut such as 70-90 is applied. Even worse, at the highest energies only neutrons are accepted, but no photons! The peculiar PSD_I distribution of D1-05 is most likely due to the fact that the PSD_0 photon and neutron peaks are very close to each other for this module, making it very hard to obtain proper fits in `IFC` and thus to correct PSD_0 properly. For other D1 modules the E1 dependence of the PSD_I distribution at the highest energies is much less pronounced.

The energy dependence of the PSD_I distributions does not allow photons to be separated from neutrons independent of energy. The best way to correct this energy dependence would be to improve `IFC` such that the fits of the PSD_0 distributions are based on more than than just the data of a single day. This approach, however, would be very time consuming. In additon, it is not clear that the benefits could justify the required amount of work. Therefore a much simpler and quicker approach was adopted. Empirical corrections of the

[2]The PSD value is a measure for a combination of the rise and decay times of the scintillation light pulse in D1 (John Macri, UNH, private communication).

PSD_I distributions were determined such that the separation of photons and neutrons is as independent of energy as possible. In the following, the corrected PSD_I values are denoted by PSD_{II}. The PSD_{II} distribution as a function of E1 for D1 module 5 is depicted in the top right panel of Fig. 3. The empirical corrections are (with E1 in [MeV]):

- **D1-01:** no correction
- **D1-02:** for E1>10 MeV:
  $PSD_{II} = PSD_I - 0.5 \cdot E1 + 5$
- **D1-03:** for E1>12 MeV:
  $PSD_{II} = PSD_I - 1.25 \cdot E1 + 15$
- **D1-04:** for E1>8.6 MeV:
  $PSD_{II} = PSD_I + 0.0234 \cdot (E1 - 14.219)^3 - 0.34077 \cdot (E1 - 14.219) + 2.2123$
- **D1-05:** for E1>6 MeV:
  $PSD_{II} = PSD_I + 0.043541 \cdot (E1 + 12.676)^2 - 15.12$
- **D1-06:** no correction
- **D1-07:** same as D1-02

To address the question of a possible time dependence of these PSD_I corrections the PSD_I distributions for individual Observation Periods from Phases 1 through 6 were compared. No significant deviations could be found within the available statistics. Therefore it is assumed that the PSD values are indeed extremely stable and that the PSD_I corrections are independent of time.

The combined PSD_I and PSD_{II} distributions of all D1 modules for E1>2 MeV are shown in the bottom left and right panels of Fig. 3, respectively. For PSD_I the photon and neutron distributions are somewhat blurred at the highest E1 energies, rendering a separation difficult. For PSD_{II} the two distributions are more clearly separated, allowing a cleaner separation between photons and neutrons at these high E1 energies. The combined PSD_I distribution of all D1 modules for E1 between 70 keV and 2000 keV is shown in Fig. 4 (note that at these low E1 energies the PSD_I and PSD_{II} values are identical).

As can be seen from Fig. 4 and the left panel of Fig. 5, the standard PSD selection of 0-110 is not the best choice. This standard selection does not reject the "artifacts" at low PSD values for E1 below about 1 MeV. More important, with increasing energy an increasing fraction of all accepted events is due to neutrons. This problem, however, can easily be solved by introducing an E1 dependent PSD selection. The goal of this energy dependent selection should be to accept as many photons as possible while rejecting as many neutrons as possible. From the PSD_{II} distributions in Figs. 3 and 5 the following E1 dependent PSD_{II} ranges seem to be reasonable:

- E1 = 70 keV: 40 - 110

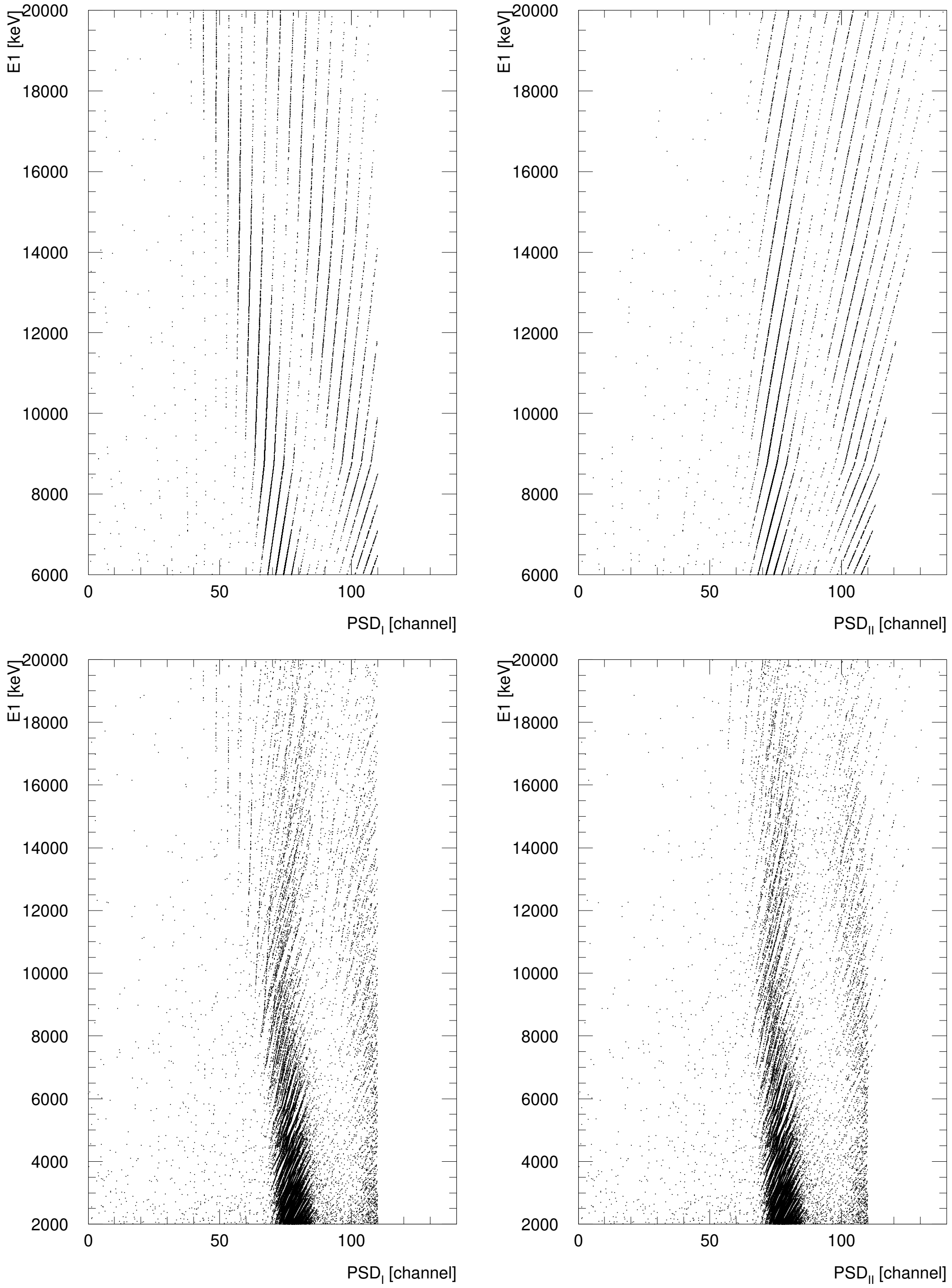

Figure 3: **Top left:** *The PSD_{I} distribution of D1-05.* **Top right:** *The PSD_{II} distribution of D1-05.* **Bottom left:** *The PSD_{I} distribution of all D1 modules.* **Bottom right:** *The PSD_{II} distribution of all D1 modules.*

- E1 = 1 MeV: 55 - 95
- E1 = 10 MeV: 55 - 92
- E1 = 20 MeV: 40 - 90

At intermediate energies these ranges are interpolated linearly. The low value of $PSD_{II,\,low}$ at the highest E1 energies is due to a peculiarity of D1 module 1: the lower boundary of its photon PSD distribution decreases from about 60 channels to about 40 channels for E1 energies between 10 MeV and 20 MeV.

In their re-analysis of the COMPTEL event selections for the energy range 10-30 MeV (*Improved COMPTEL 10-30 MeV Event Selections for Point Sources from Inflight Data*, Proc. of the 4. Compton Symposium, 1997) W. Collmar et al. concluded that a PSD_I selection of 65-85 might be best. This selection, however, was derived from studying the Crab signal as function of the PSD_I range only and did not include a study of the detailed correlation between E1 and PSD_I. As can be seen in Figs. 3 and 5, a PSD_I range of 65-85 is very "tight" and does reject a small fraction of photon events - which is also true for PSD_{II}. At present, it is not possible to take this into account properly in the telescope response, for the simple reason that there is no PSD calibration data for E1$>$ 1630 keV. This problem does not occur with the E1 dependent PSD_{II} selection, as can be seen in Figs. 3 through 5. An additional check of the E1 dependent PSD_{II} selection is depicted in Fig. 5. The left panel shows the PSD_{II} distribution of the data used in the analysis by W. Collmar et al., the right panel shows the same data with an additional ARM cut from -2.5° to 2.5° on the Crab, representing to a good approximation the PSD_{II} distribution of celestial photons. Within the available statistics both photon distributions are identical, as expected (there might be a difference at the lowest energies, where the neutron distribution disappears (!), but this needs to be studied in more detail), showing that the E1 dependent PSD_{II} selection rejects most neutrons while rejecting at most a negligible fraction of the signal - which is exactly what the PSD selection is supposed to do.

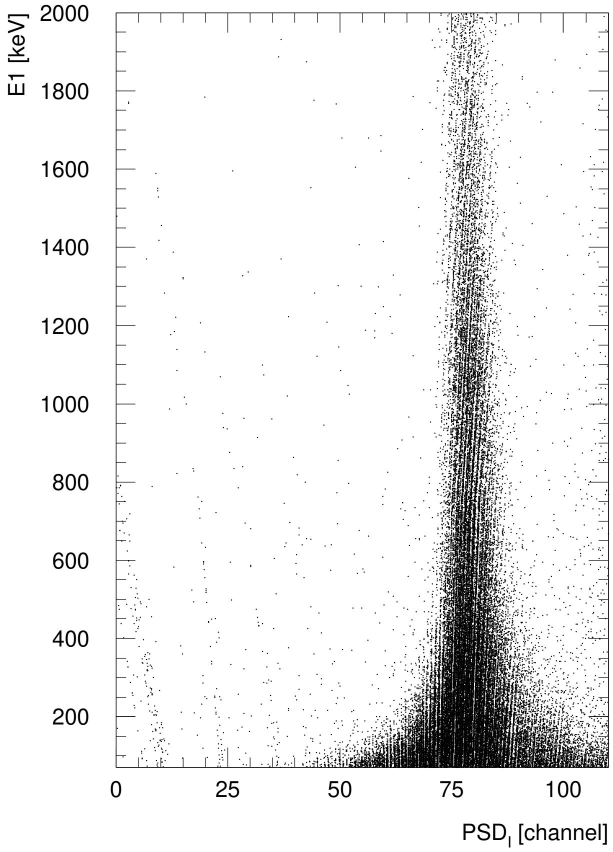

Figure 4: *The combined PSD$_{\rm I}$ distribution of all D1 modules for E1 between 70 keV and 2000 keV. At these low energies the PSD$_{\rm I}$ and PSD$_{\rm II}$ values are identical.*

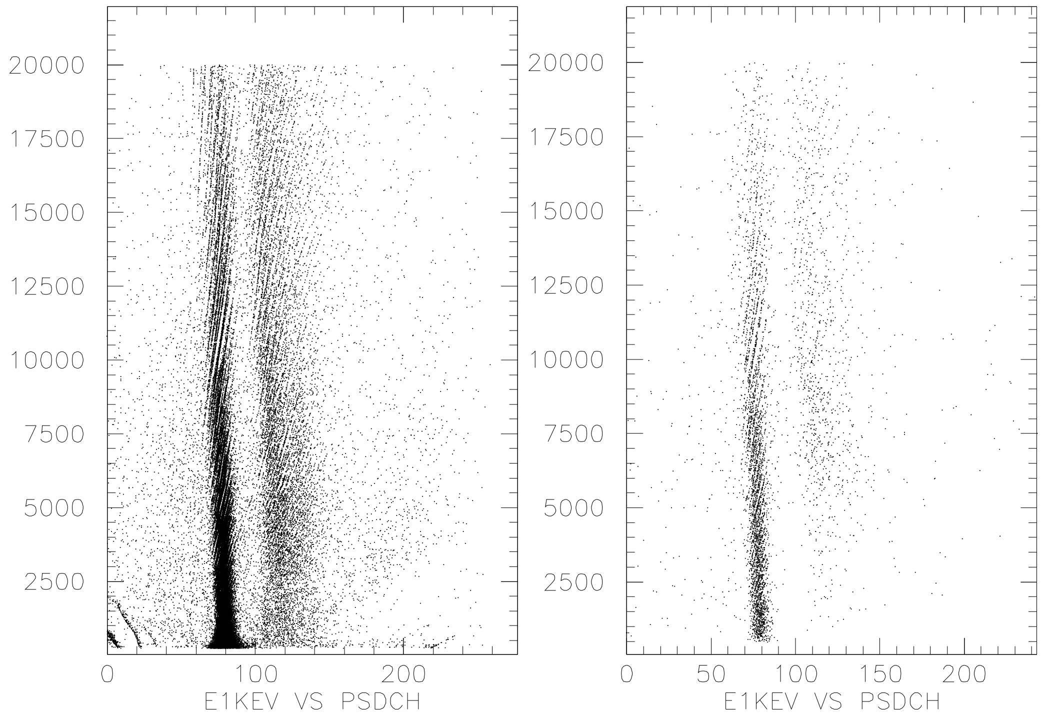

Figure 5: **Left:** *The combined "Crab data" PSD$_{\rm II}$ distribution of all D1 modules for $E_{\rm tot} < 7$ MeV.* **Right:** *The same data, with an ARM cut from -2.5° to 2.5° on the Crab.*

4 EVPTPC

The task EVPTPC has been written to make the ToF and PSD corrections available within COMPASS. The required input consists of an EVP-132 dataset (no lists are accepted), a TCC dataset and a FPM dataset.

The TCC dataset contains the ToF correction coefficients. At present, we recommend using M-TCC-5 which contains the ToF correction coefficients for D2-01 and D2-03 through D2-14, with D2-11, 13 and 14 each having one failed PMT. EVPTPC checks the valid module status according to the database table SBM.MODULE_ONOFF against the module statuses that can be corrected with the input TCC data. If there is an inconsistency, for example the status of D2 module 11 is 1 when using M-TCC-5, then EVPTPC will be aborted. If M-TCC-5 is used, all EVP datasets after TJD 8654 in OP 19 can be improved. In addition, only those events that could be corrected are written to the output EVP dataset. Thus events from modules with module status 0, from D2-02, and from those areas rejected from D2 modules 11, 12 and 14 are *not* written to the output EVP dataset which, for the time being, are assigned a quality flag of 68.

The FPM dataset describes those regions of the D2 modules 11, 13 and 14 which have be to excluded due to the failed PMTs.

The only output of EVPTPC is an EVP dataset. Apart from the ToF and PSD values all event parameters of the events written to the output EVP dataset are identical to those in the input EVP-132 dataset.

5 Comparisons

For a first, preliminary comparison of corrected and standard `EVP` data OPs 511 and 511.5 were used, in which 3C 279 was observed in a flaring state (the EGRET results were published by A. Wehrle et al., *Multiwavelength Observations of a Dramatic Flare in the Blazar 3C 297*, ApJ, submitted, 1997; the COMPTEL results were published by W. Collmar et al., *Evidence for γ-Ray Flares in 3C 279 and PKS 1622-297 at $\sim$10 MeV*, Proc. of the 4. Compton Symposium, 1997). This comparison was performed in two energy ranges: 4.3-9 MeV and 10-30 MeV. The standard `EVP-131` data was processed with the standard `EVP-131` selection set `MPE006`. For the corrected `EVP` data the PSD selection of Sec. 3 and an energy dependent ToF selection (4.3-9 MeV: 117.25-126.5, 10-30 MeV: 116.5-123.25) was used[3]; all other selections were identical to `MPE006`. In addition, in the 10-30 MeV range the standard `EVP-131` data was processed with the PSD and ToF selections of W. Collmar et al. (*Improved COMPTEL 10-30 MeV Event Selections for Point Sources from Inflight Data*, Proc. of the 4. Compton Symposium, 1997): PSD 65-85, ToF 113-126, all other selections as in `MPE006`. All `MLM` maps compared in the following were generated with `SRCLIX`, using the standard background method 'A' and the standard PSFs for 3-10 MeV and 10-30 MeV.

The 10-30 MeV MLM maps obtained for the standard `EVP-131` data with the standard `MPE006` selection set, the standard `EVP-131` data with the selections of W. Collmar et al. and the corrected `EVP` data with the PSD and ToF selections given above are depicted in Figs. 6, 7 and 8, respectively. In all maps the same color coding and contour levels (6 step 3) for the MLR values were used. The triangle indicates the position of 3C 279, the circle marks the location of 3C 273. The standard map does not show any significant source-like feature and appears to be more dominated by "artifacts" than the other two maps - despite the fact that it was derived from the largest number of events. In marked contrast, the other two maps clearly show a source feature at the position of 3C 279. In addition, these two maps seem to be "cleaner" than the standard map. The highest significance for the quasar is obtained with the corrected `EVP` data. A more quantitative comparison of the three maps is given in Table 1, which summarizes the number of events contained in each map, the MLR values and the significance at the positions of the two quasars (assuming one degree of freedom), and their fluxes (including ToF correction factors) as derived from a combined fit.

The 4.3-9 MeV MLM maps obtained for the standard `EVP-131` data with the standard `MPE006` selection set and the corrected `EVP` data with the PSD and ToF selections given above are shown in Figs. 9 and 10, respectively[4]. Again, the standard map and the map obtained with the corrected `EVP` data are markedly different. The standard map is dom-

[3]The derivation of these ToF ranges, based on the maximization of the S/N ratio as inferred from ToF spectra from **completely independent** data, will be explained in detail in *Studying the ToF Spectrum as a Function of Energy Part 3: the Forward Peak Region above 4.3 MeV* (`COM-RP-MPE-175`) by G. Weidenspointner, M. Varendorff and W. Collmar, which also explains why the 4.3-9 MeV band was used.

[4]W. Collmar et al. could only improve the standard selections above 10 MeV.

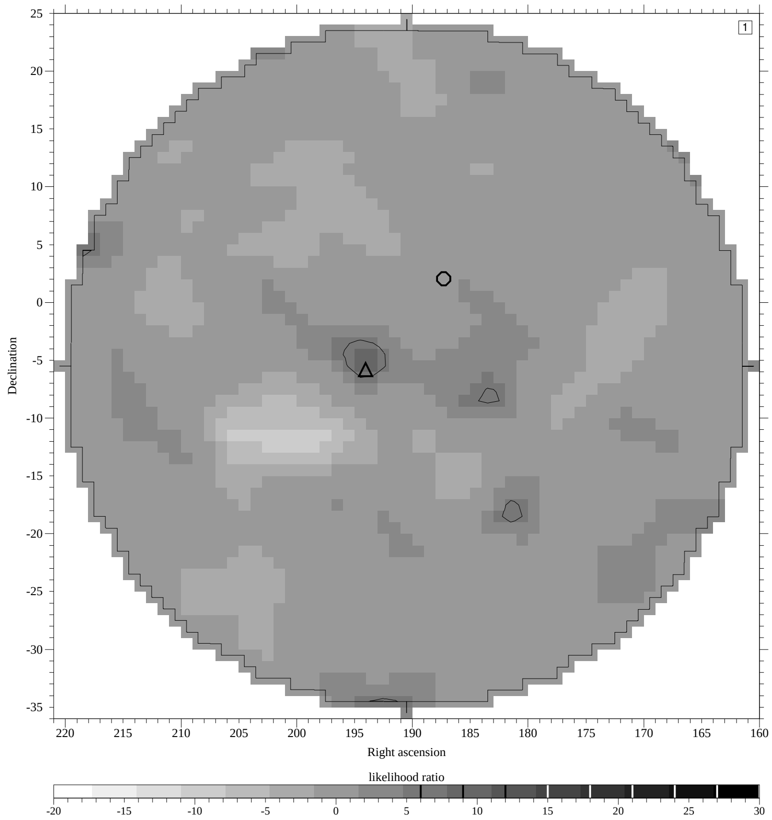

Figure 6: *10-30 MeV standard MLM map derived with the standard* `EVP-131` *data, the standard selection set* `MPE006` *and the standard 10-30 MeV PSF.*

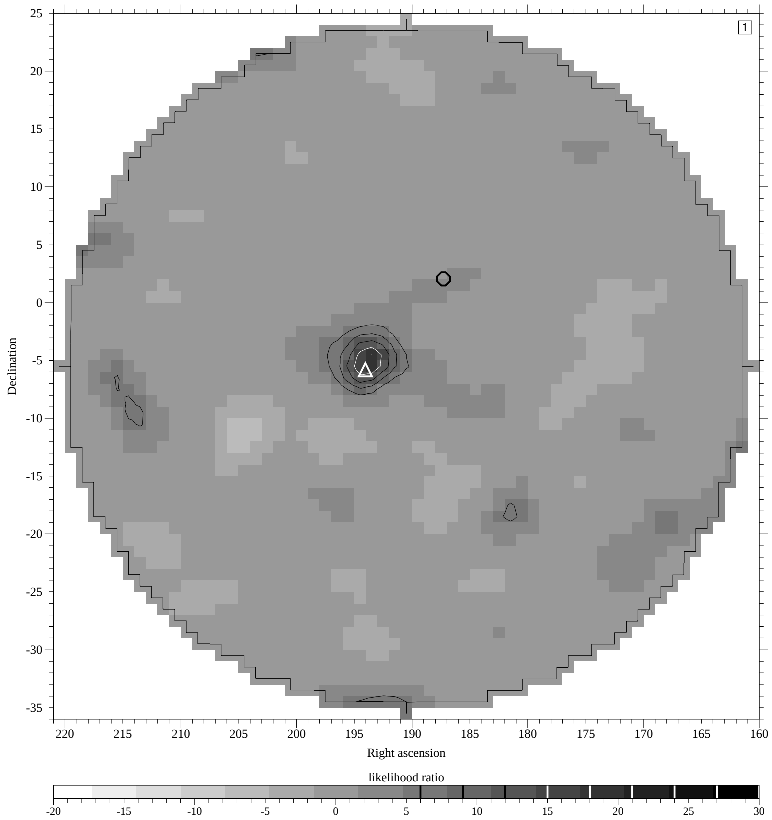

Figure 7: *10-30 MeV MLM map derived with the standard* `EVP-131` *data, the selections of W. Collmar et al. and the standard 10-30 MeV PSF.*

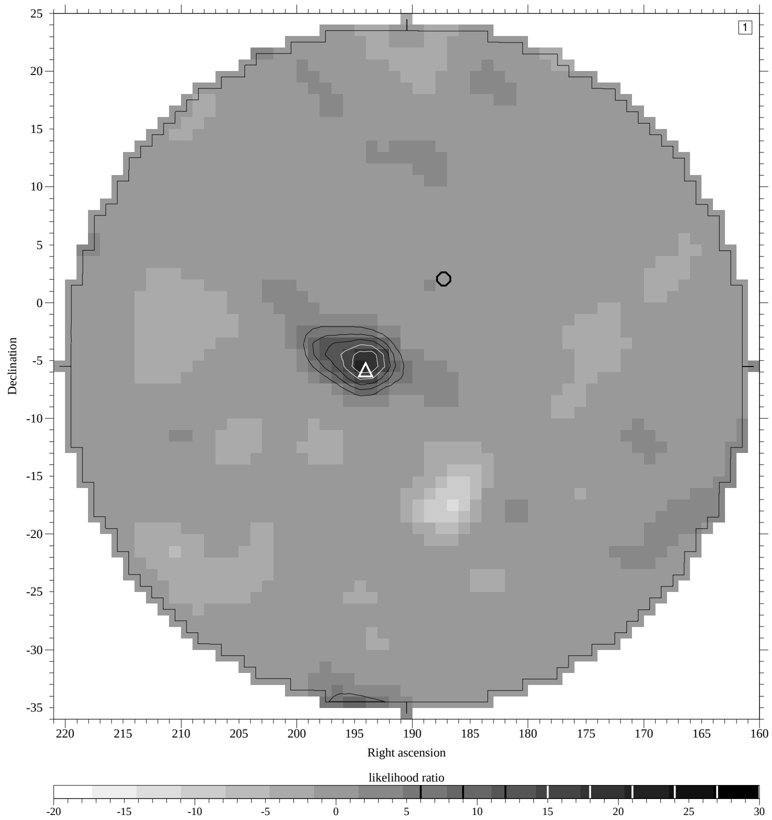

Figure 8: *10-30 MeV MLM map derived with the corrected* `EVP` *data, the ToF and PSD selections described above and the standard 10-30 MeV PSF.*

inated by a significant, somewhat extended feature centered about 3° off the position of 3C 273. This feature extends down to 3C 279, which is not really detected. Two other features, supposedly artifacts, are more significant than the latter quasar. Using the corrected `EVP` data and the ToF and PSD selections described above, two source features of reduced significance close to the positions of the two quasars appear instead of the more significant, but extended source feature off 3C 273. Moreover, this map seems to be cleaner than the standard map. A quantitative comparison of the two maps is summarized in Table 2.

If the maps obtained with the corrected `EVP` data could be taken at face value, then it would be possible to repeat this analysis in a finer energy binning. Assuming for the moment that this is the case, the resulting energy spectra for 3C 273 and 3C 279 are depicted in the top and bottom panel of Fig. 11. These data points are represented by circles. In this analysis the existing 4.0-5.6 MeV and 5.6-10 MeV PSFs were used for the 4.3-6 MeV and 6-9 MeV energy bands, respectively, in 9-12 MeV the standard 10-30 MeV PSF was used, and above 12 MeV the existing 12-30 MeV PSF was used. The squares are the result of the standard analysis according to W. Collmar et al.: below 10 MeV they were derived using standard `EVP-131` data, standard selections, PSFs and energy binning, in the 10-30 MeV band the selections of W. Collmar et al. were used (a standard analysis returns at best fluxes of marginal significance above 10 MeV). It seems that the fluxes derived in these analyses are consistent with each other. In addition, the corrected `EVP`

EVP data	standard EVP	standard EVP	corrected EVP
EVP selection	MPE006	W. Collmar et al.	this report
events in map	13377	9829	7618
3C 273 MLR value	0.2	1.6	1.0
3C 279 MLR value	8.5	17.3	20.8
3C 273 significance (1 dof)	0.4 σ	1.3 σ	1.0 σ
3C 279 significance (1 dof)	2.9 σ	4.2 σ	4.6 σ
3C 273 flux [10^{-4}/cm^{2}sec]	0.052 ± 0.066	0.087 ± 0.096	0.060 ± 0.057
3C 279 flux [10^{-4}/cm^{2}sec]	0.185 ± 0.066	0.256 ± 0.063	0.254 ± 0.059

Table 1: *Comparison of the three 10-30 MeV MLM maps.*

EVP data	standard EVP	corrected EVP
EVP selection	MPE006	this report
events in map	83496	56274
3C 273 MLR value	15.9	10.0
3C 279 MLR value	3.8	6.6
3C 273 significance (1 dof)	4.0 σ	3.2 σ
3C 279 significance (1 dof)	2.0 σ	2.6 σ
3C 273 flux [10^{-4}/cm^{2}sec]	0.491 ± 0.124	0.347 ± 0.108
3C 279 flux [10^{-4}/cm^{2}sec]	0.262 ± 0.121	0.305 ± 0.106

Table 2: *Comparison of the two 4.3-9 MeV MLM maps.*

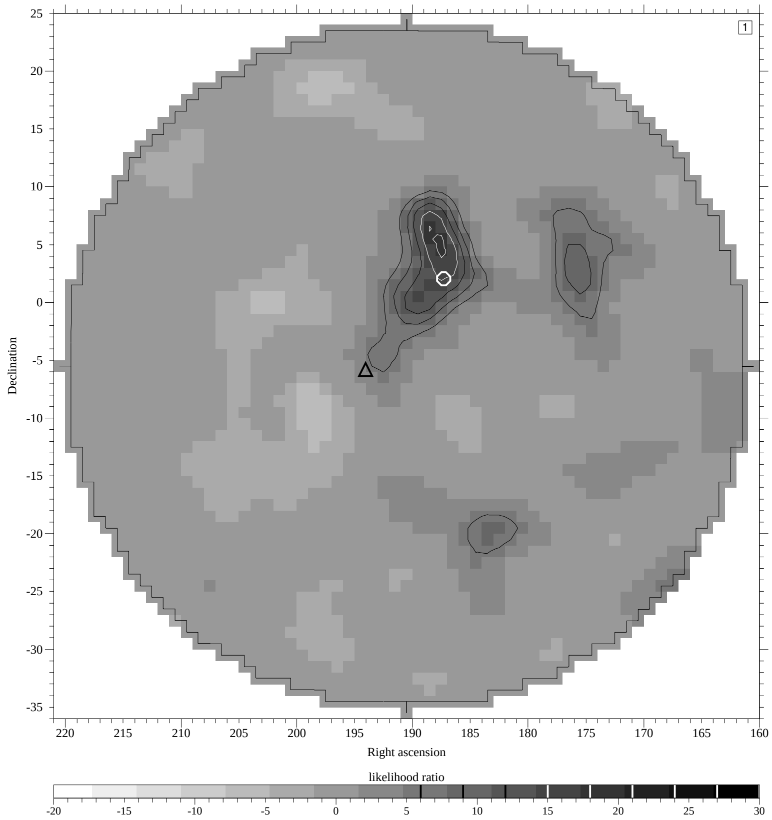

Figure 9: *4.3-9 MeV standard MLM map derived with the standard* `EVP-131` *data, the standard selection* `MPE006` *and the standard 3-10 MeV PSF.*

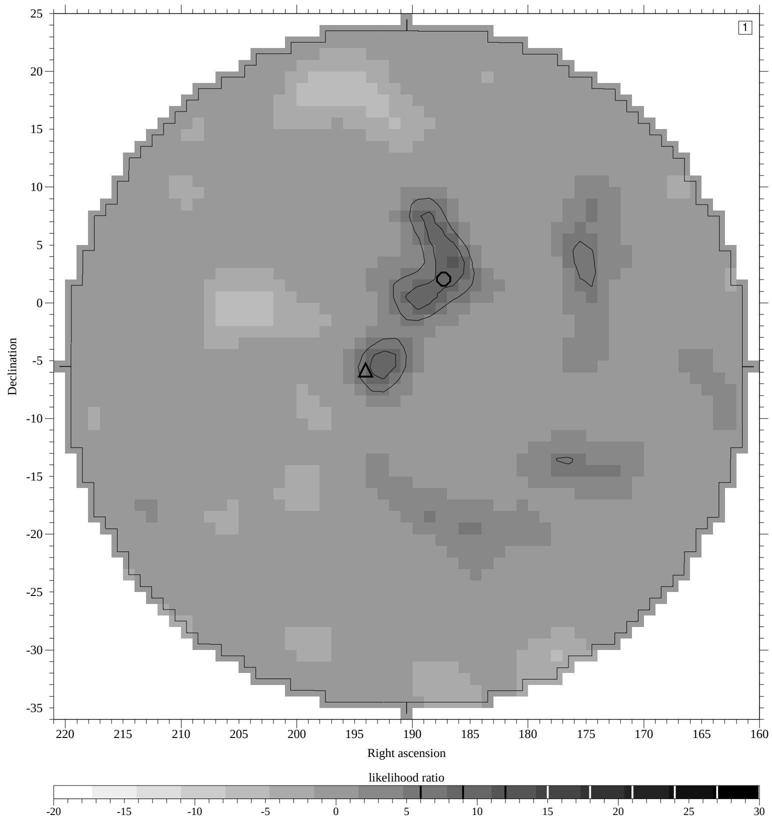

Figure 10: *4.3-9 MeV MLM map derived with the corrected* `EVP` *data, the ToF and PSD selections described above and the standard 3-10 MeV PSF.*

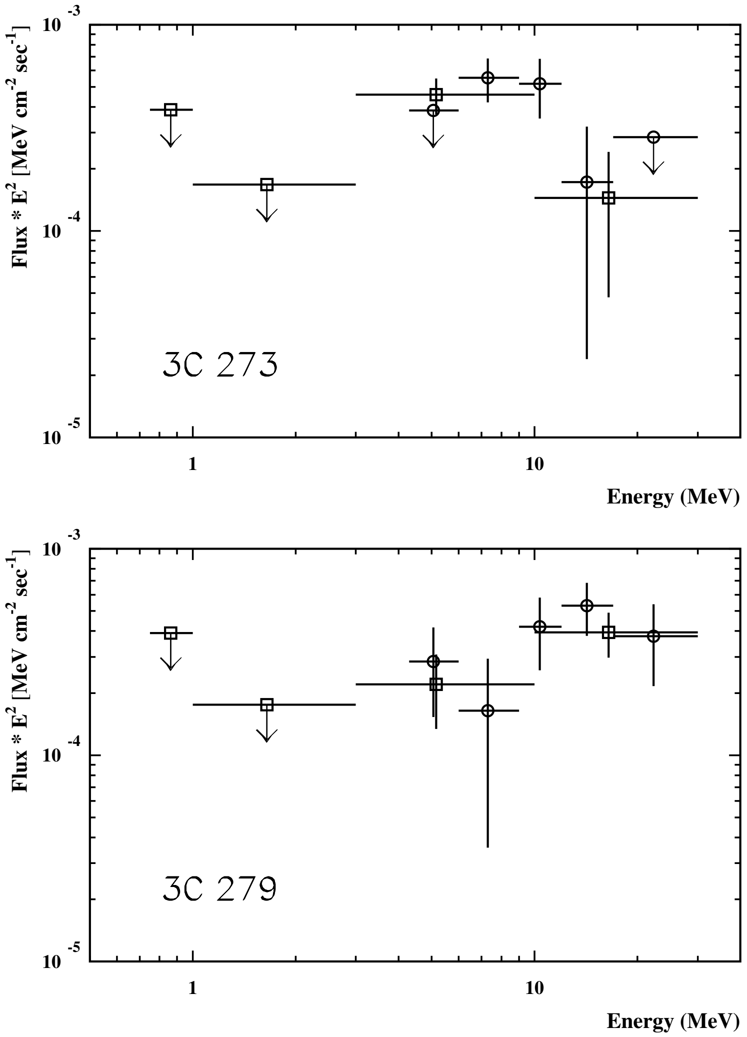

Figure 11: *The energy spectra of 3C 273 (top) and 3C 279 (bottom) as derived with the corrected* `EVP` *data, represented by the circles. The squares were obtained from a standard analysis: standard below 10 MeV and according to W. Collmar et al. above 10 MeV. 2σ upper limits are plotted if the flux is less than the 1σ error.*

data seems to allow us to work with finer energy bins. In the case of 3C 279 there is no qualitative change of the overall spectrum. In the case of 3C 273, however, the spectrum now is more similar to an MeV-Blazar spectrum than before.

These preliminary results obtained with different sets of `EVP` data and different selection sets are not sufficient to decide on the "quality" of different kinds of `EVP` data or selection sets. The selections of W. Collmar et al. and the selections derived for the corrected `EVP` data are both intended to maximize the number of "source events" relative to the number of "background events", based on the assumption that this will facilitate the detection of any kind of source-like (cone-like) structure in the data space. All that can be said at the moment is that it seems easier for `SRCLIX` to find point sources when the S/N ratio is increased. In addition, the 10-30 MeV maps indicate that `SRCLIX` might "prefer" the corrected `EVP` data over the standard `EVP-131` data. Work is in progress to address these questions by attempting to disentangle the effects of different kinds of `EVP` data and different selection sets.